

## Tomographic reconstruction from energy-filtered images of thick biological sections

by ADA L. OLINS, DONALD E. OLINS, HENRI A. LEVY\*, STEPHEN M. MARGLE†, ED P. TINNEL†, and RICHARD C. DURFEE†, *The University of Tennessee-Oak Ridge Graduate School of Biomedical Sciences, and Biology Division, \*Chemistry Division, Oak Ridge National Laboratory, P.O. Box 2009 and \*P.O. Box 2008, and †Computing and Telecommunications Division, Martin Marietta Energy Systems, Inc., P.O. Box 2009, Oak Ridge, TN 37831, U.S.A.*

**KEY WORDS.** Electron microscope tomography, energy filtration, energy spectroscopic imaging, thick sections, eukaryotic chromosome transcription.

### SUMMARY

Energy filtration makes it possible to image a  $\sim 0.5 \mu\text{m}$  biological section at 80 kV in the electron microscope. Based on spectra taken at different tilt angles, we chose the most probable energy loss,  $\Delta E_p \pm 10 \text{ eV}$  for each tilt angle, as the imaging energy window. A complete tilt series from  $+60^\circ$  to  $-60^\circ$  at  $2.5^\circ$  intervals was collected on the Zeiss EM902 and used in a tomographic reconstruction of transcriptionally active chromatin in the Balbiani ring of *Chironomus tentans*.

### INTRODUCTION

Three-dimensional (3-D) visualization and analysis of thick (i.e.  $> 0.25 \mu\text{m}$ ) plastic sections is an area of considerable interest to cell biologists. Even at low resolution (e.g. 10–20 nm) the complex paths and structural relationship of cellular components, such as chromatin fibres or microtubular arrays, must be elucidated in order to understand functional mechanisms. Electron microscopists have generally employed two different methods for the analysis of large volumes of cellular space: serial reconstruction of ultrathin (i.e. 30–50 nm) sections; and stereo microscopy of thick sections viewed in high or intermediate voltage (HVEM, IVEM) electron microscopes (for a compilation of articles on these approaches, see Turner, 1981).

The newer method of electron microscope tomography (EMT), which combines tilted projections of asymmetric ultrastructures to generate a computed 3-D electron density matrix (Hoppe & Hegerl, 1980; see Olins *et al.*, 1983 for method and earlier references), has recently been applied to sections  $0.25\text{--}0.75 \mu\text{m}$  thick, employing HVEM and IVEM (McEwen *et al.*, 1986; Olins *et al.*, 1986; Belmont *et al.*, 1987).

The development of electron energy filtering techniques (Castaing & Henry, 1962) and their installation on modern electron microscopes constitutes a major advance which can be exploited for the 3-D reconstruction of thick sections. The new Zeiss EM902 with 'electron spectroscopic imaging' yields excellent quality images of stained

thick sections at 80 kV (Bauer, 1987; Heath & Peachy, 1987). The present paper demonstrates that EMT of thick sections can be conveniently performed using energy-filtered images. In order to establish the validity of using these images in a reconstruction we undertook a collaborative study (Colliex *et al.*, 1989), in which data collected on a dedicated STEM VG-HB501 with a sophisticated data collection interface, was quantitatively analysed. A brief discussion of the considerations involved in optimizing image data collection, derived from the quantitative analysis, is included within this study. Results from the Zeiss EM902 are essentially equivalent to our previous work using an IVEM at 300 kV (Olins *et al.*, 1986), suggesting that the energy-filtered image is adequately linear for purposes of reconstruction (DeRosier & Klug, 1968).

## MATERIALS AND METHODS

### 1. Specimen

Data collection was performed on a thick (i.e. approximately 0.5  $\mu\text{m}$ ) embedded stained section. The object of interest to reconstruct was a Balbiani ring 2 (BR2) located on the fourth polytene chromosome of the salivary gland of *Chironomus tentans*. We have previously described these materials and preparation of stained sections (Olins *et al.*, 1984, 1986). The BR2 genes are known to be the sites of synthesis of a 37 kb mRNA that is translated into a protein of mol. wt approximately  $10^6$  Da. The nascent RNA is coiled into distinctive ribonucleoprotein particles of 45–50 nm diameter, the BR granules, whose 3-D folding and internal structure is also being examined by EMT (Skoglund *et al.*, 1986). Our interest in 3-D reconstruction of the BR2 genes is directed at describing the *in situ* arrangement of the nascent transcripts along the DNA axis in single transcription loops as a step towards understanding DNA compaction in chromosomes during intense transcription. The thick section was obtained from salivary glands (made hyperactive by pilocarpine-stimulation), glutaraldehyde-fixed, post-fixed with  $\text{OsO}_4$ , *en bloc*-stained with uranyl acetate, embedded in Epon, sectioned, stained with uranyl acetate and lead citrate and lastly, colloidal gold particles adsorbed to both surfaces of the section to provide control points for alignment and registration of the many projected images.

### 2. Microscopy

Since the top-entry tilt stage of the Zeiss EM902 is not eucentric, the grid was rotated within the holder in order to bring a BR2 onto the tilt axis. The procedure involved repeated cycles of rotating and tilting the grid until the objective lens current to achieve focus was the same at any tilt angle. Since small changes in the objective lens current could not be read, the number of objective lens control clicks between focus at two constant tilt angles indicated the direction of grid rotation needed to bring the area of interest on the tilt axis.

Energy (eV)-loss spectra (Fig. 1) were collected on an adjacent region of cytoplasm in one tilt direction at the following angles: 0, 10, 20, 30, 40, 45, 50, 55 and 60°. Instrumental parameters during spectral analysis were the following: 30  $\mu\text{m}$  objective aperture, 20 eV window, 80 kV primary beam. Peak positions, i.e. the most probable energy loss ( $\Delta E_p$ ) of the energy loss spectra (intensity versus energy loss) were estimated by eye and a plot of  $\Delta E_p$  versus the reciprocal of the cosine of the tilt angle (the effective thickness) was prepared (Fig. 2).

For image collection the spectrometer slit width was set at 20 eV, and positioned at  $\Delta E_p$ . The microscope automatic exposure feature was employed; images were recorded on film. Fifty-one projections were collected at a magnification of 6000 including three at 'nominal zero degrees' taken before, midway and at the end of the tilting procedure; the average angular difference between successive projections was approximately 2.5°.

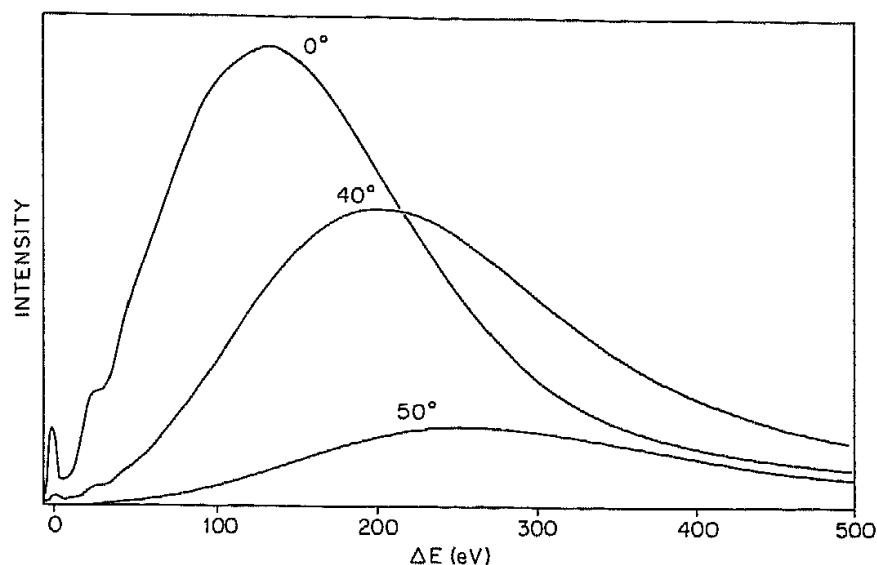


Fig. 1. Three sample energy loss spectra of a region of the cytoplasm taken near the nucleus containing the Balbiani ring which was reconstructed in this paper. The ordinate is proportional to the intensity or number of electrons and the abscissa represents the energy loss of the electrons.

### 3. Alignment and reconstruction

The entire set of micrographs and an image of a calibration grid were digitized as described previously (Olins *et al.*, 1983, 1984, 1986) employing a vidicon camera interfaced to an  $I^2S$  image processing system. Each digitized image has a  $512 \times 512$  pixels spatial resolution and a 256 grey level resolution, with the pixel size set at 10 nm, based upon the image of the calibration grid. The alignment and registration program combines the coordinates of selected gold particles on each projection to calculate a least-squares single tilt axis ( $Y$ ). Tilt angles were calculated, as well as magnification of each projection relative to the initial untilted micrograph (the maximum magnification change was 1.7%, most were different by less than 1.0%). The images were all computationally translated and rotated from  $7.4$  to  $10.8^\circ$  depending upon the projection, to bring them into coincidence, and make the tilt axis vertical. This procedure resulted in minor areas of missing data at the boundaries of the reconstruction, which produced striations within each slice of the final reconstruction.

## RESULTS

Typical energy-loss spectra (intensity versus eV) at several tilt angles are presented in Fig. 1. Even at a  $0^\circ$  tilt, the number of zero-loss electrons is small relative to the inelastically scattered electrons for this particular specimen. With increasing tilt, and effectively increased thickness, the intensity of zero-loss electrons becomes negligible (obviously insufficient for imaging), the intensity maximum shifts to higher energy loss values and the total number of electrons observed to penetrate the specimen and pass the objective aperture decreases. The shift of the intensity maximum position ( $\Delta E_p$ ) is linear with increased thickness, if the composition of the specimen is not changed (Fig. 2 and see Discussion). The first and second plasmon peaks ( $\Delta E = \sim 25$  and  $50$  eV, respectively) can be discerned in the  $0^\circ$  tilt angle spectrum.

A physical and mathematical interpretation of such eV-loss spectra from thick sections is given by Colliex *et al.* (1989). Since the collection of data for this reconstruction preceded the quantitative study, we chose to collect the tilt series with a 20 eV window centred at  $\Delta E_p$ . These conditions maximized the intensity of elec-

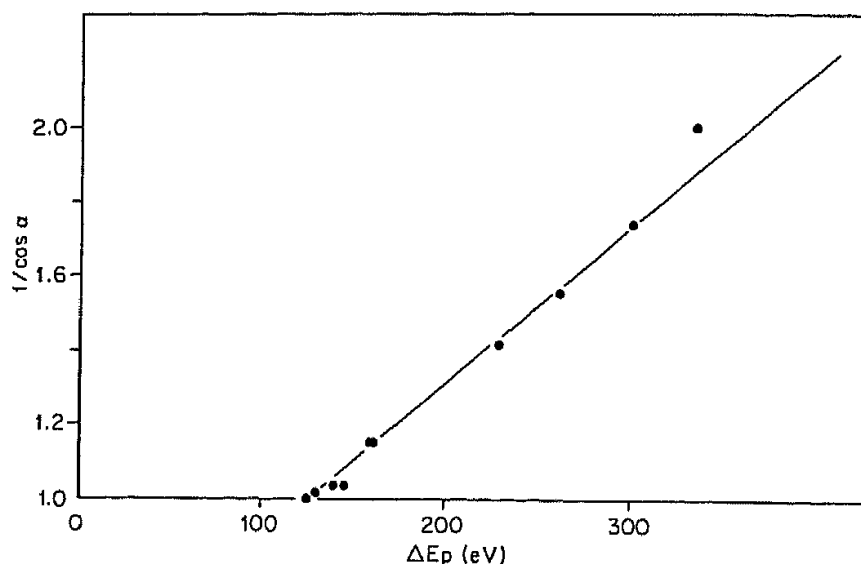
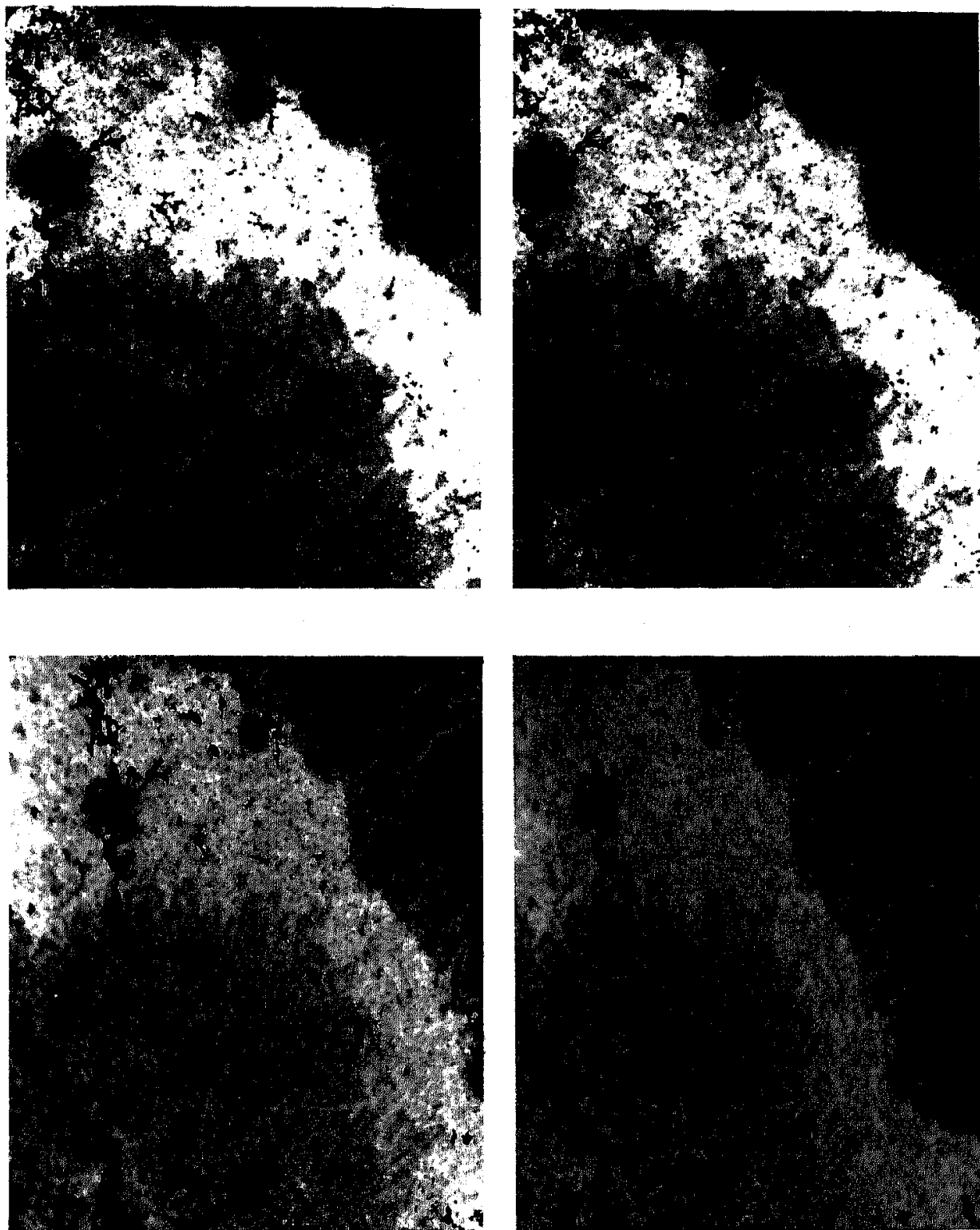


Fig. 2.  $\Delta E_p$  (abscissa), the most probable energy loss, is the position of maximum intensity taken from spectra such as those shown in Fig. 1. All spectra were taken in the same specimen region at different tilt angles. The ordinate is  $(1/\cos \alpha) = (t/t_0)$  where  $t_0$  is the section thickness and  $t$  is the thickness that must be penetrated by the electron beam when the section is tilted by an angle  $\alpha$ .

trons used to form the image and avoided the chromatic aberrations normally introduced by the inelastic scattering of thick sections. Furthermore, this eV window is well below the point of contrast reversal, thus forming a bright field image (see Discussion).

Several of the tilt projections are presented in Fig. 3 as two stereo pairs. We call attention to the remarkable clarity of the high tilt projections. Even at  $60^\circ$  the gold particles have sharp edges and the BR2 transcription loops are well discerned, especially in the central region of the images. At high tilt angles the edge of the specimen is outside the plane of focus and the final reconstruction has optimal resolution in the regions closest to the tilt axis (midway between the right and left edges).

Figure 4 shows six of the calculated slices (tomograms) from the final reconstruction printed with contrast reversed. The tomograms shown here are 2 pixels (i.e. 20 nm) thick and viewed normal to the plane of the 'nominal'  $0^\circ$  projection. In fact it was noted after the reconstruction, upon examination of the tomograms, that the nominal zero tilt was incorrect, and that even though the tilt stage indicated  $0^\circ$  (which is assumed during the alignment and registration of the images), the specimen section was tilted at approximately  $2.9^\circ$ . This accounts, in part, for the image of the surface gold clusters present on the left margin but not on the right side of the tomograms. The persistence of the gold clusters through adjacent slices is a consequence of the elongated point-spread function in the  $Z$  direction due to the wedge of missing data between the  $60^\circ$  and  $90^\circ$  tilts and the very high inherent electron density of gold. The BR2 transcription loops (c. 200 nm diameter) are clearly visible in the individual tomograms, especially in the central region of the reconstruction. The punctate substructure along the loops represents the BR granules (c. 45–50 nm diameter). This level of resolution in the  $XY$  plane we regard as very favourable, especially as the images were photographed at a magnification of 6000. Numerous striations are apparent at the edges of the tomograms resulting from the image translations and rotations and consequent loss of data at the periphery of the projections. As determined within a small central volume of 128 pixels<sup>3</sup>, the biological information appeared to be 40–45 pixels thick, corresponding to an apparent section thickness of 0.4–0.45  $\mu\text{m}$ .



**Fig. 3.** Stereo pairs taken from the total tilt series chosen to illustrate the high quality of the image data. Top pair,  $+10^\circ$  (left),  $-10^\circ$  (right); bottom pair,  $-50^\circ$  (left),  $-60^\circ$  (right). Magnification = 6200.

#### DISCUSSION

The present investigation demonstrates that thick stained plastic sections can be imaged with good clarity up to high tilt angles by selecting a narrow window of inelastically scattered electrons using an energy selective filtering system, such as that available on a Zeiss EM902. Because the thickness of a specimen doubles as the tilt angle changes from  $0$  to  $60^\circ$ , large changes in the energy loss spectra of the transmitted

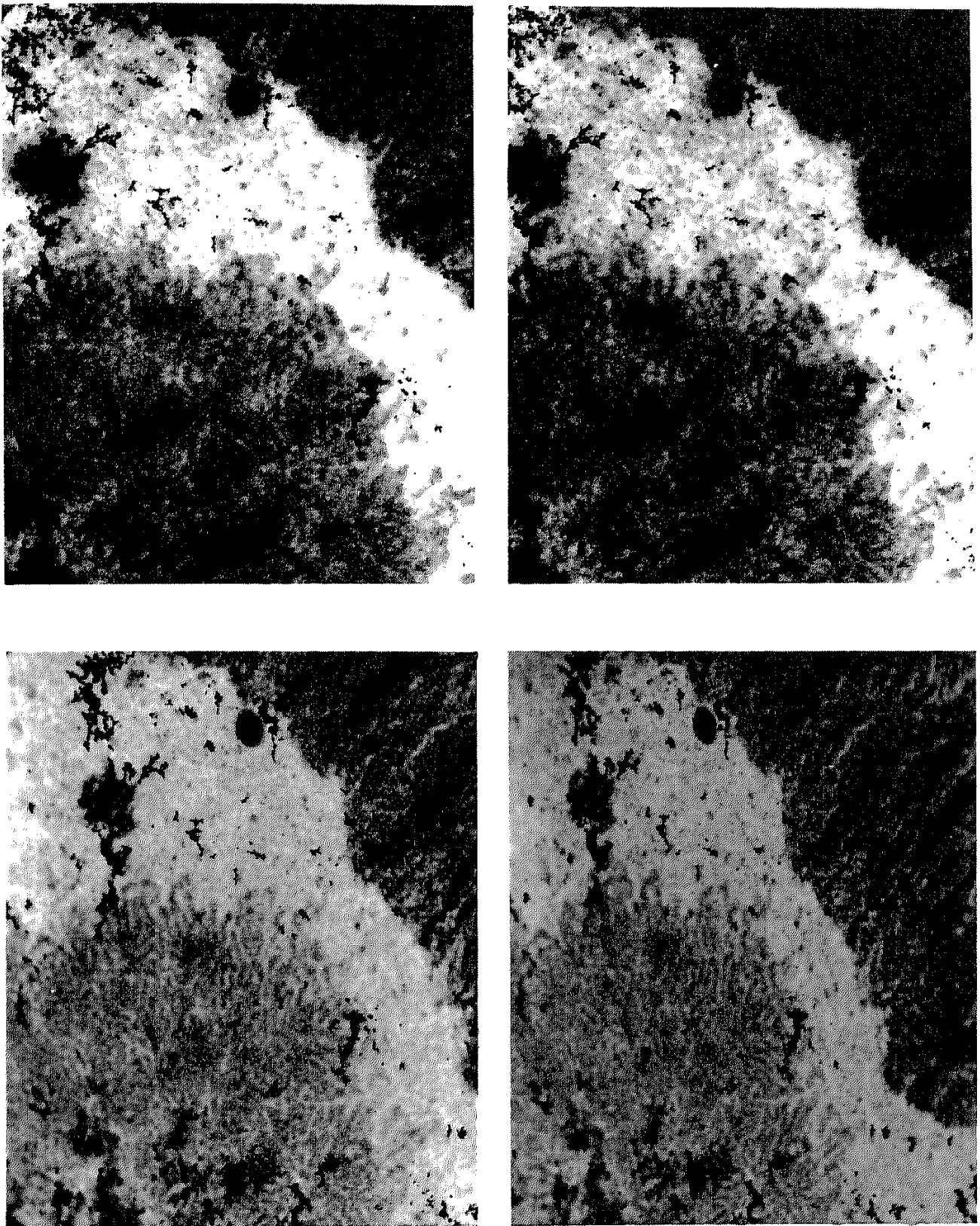
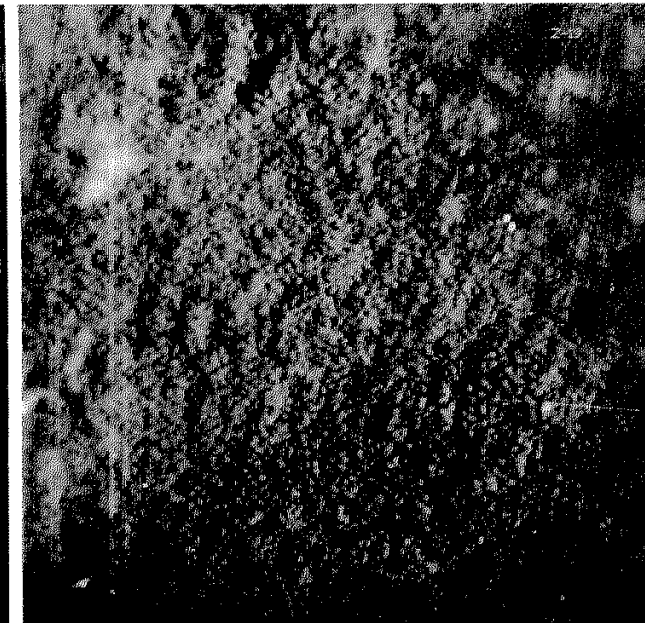
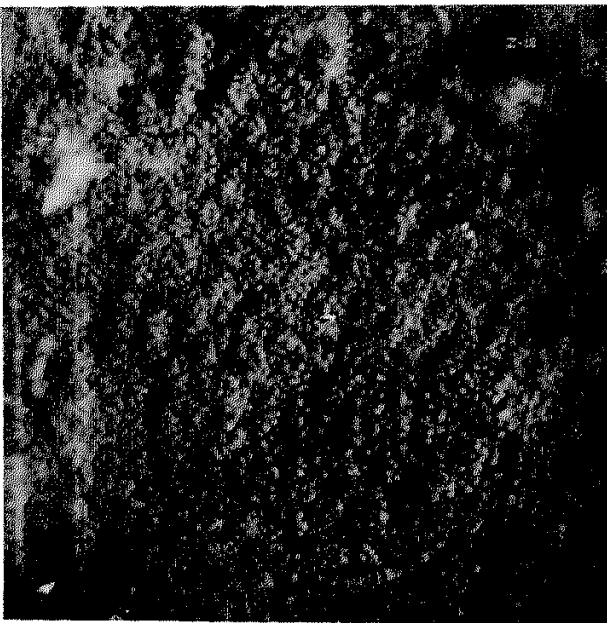
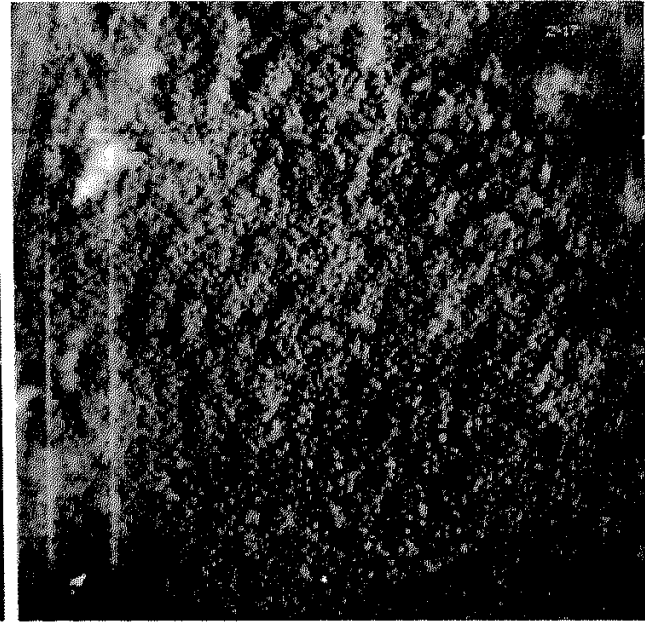
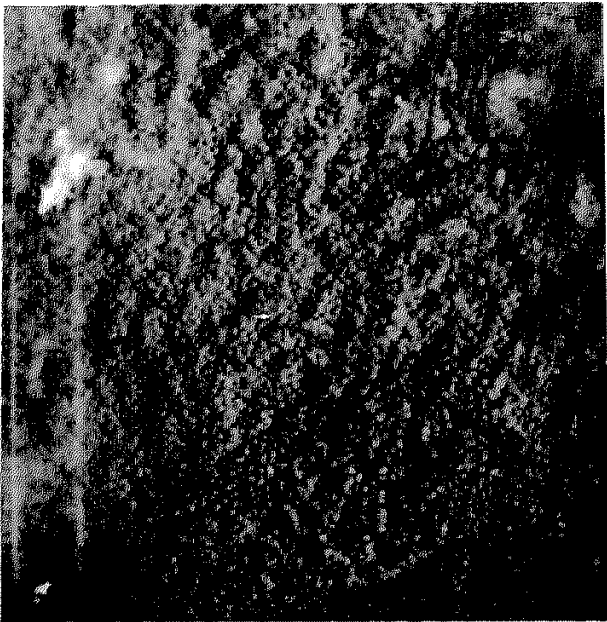
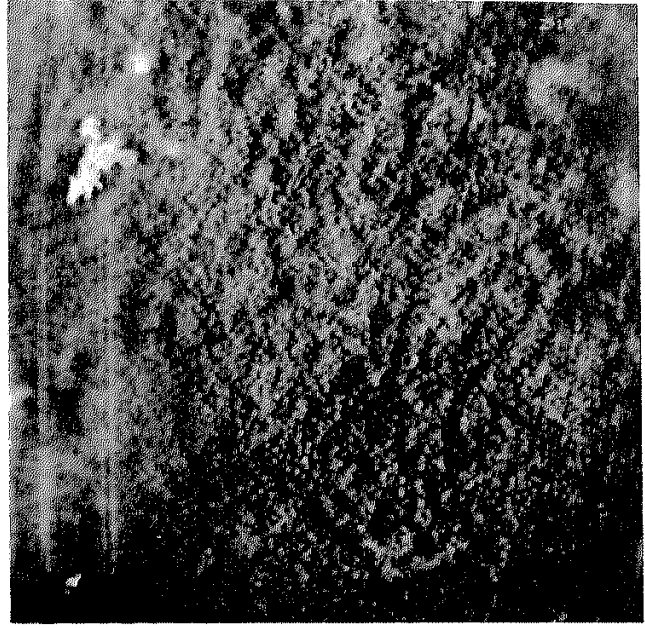
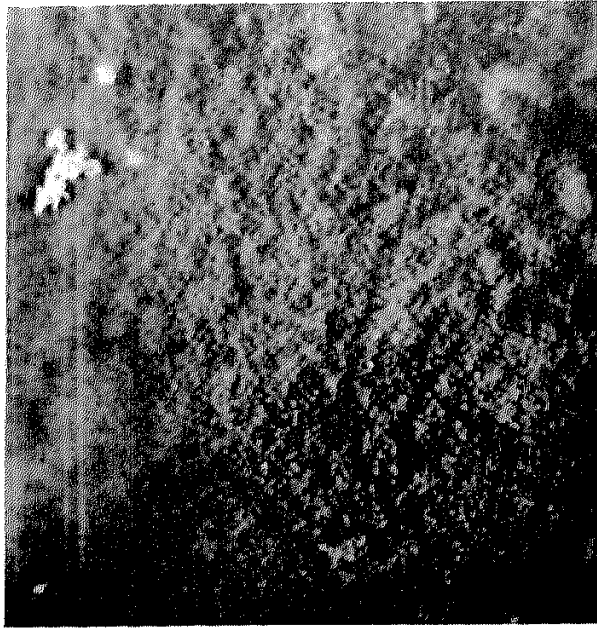


**Fig. 3.** Stereo pairs taken from the total tilt series chosen to illustrate the high quality of the image data. Top pair,  $+10^\circ$  (left),  $-10^\circ$  (right); bottom pair,  $-50^\circ$  (left),  $-60^\circ$  (right). Magnification = 6200.



electrons are observed and there are not enough zero energy loss electrons at any tilt angle to form an image. Our choice of imaging each tilt projection using electrons having the most probable energy loss for that tilt angle ( $\Delta E_p \pm 10$  eV) is soundly based on experiments and the theory of electron interaction with thick biological specimens (Colliex *et al.*, 1989 and see below) and qualitatively highly satisfactory (Fig. 3) in producing sharp images for all members of the tilt series. Thus at a  $60^\circ$  tilt, with the effective apparent thickness between 0.8 and 0.9  $\mu\text{m}$ , details in the micrograph remained sharp and clear. We were able to reconstruct this tilt series of a thick section using previously established methods (Olins *et al.*, 1983, 1984, 1986) and to demonstrate that energy filtration is a viable alternative to intermediate and high voltage electron microscopy (IVEM and HVEM). Comparison with our previous reconstruction of similar thick sections based on data collected at 300 kV without energy filtration (Olins *et al.*, 1986) indicates that both data collection methods are acceptable for stained specimens. Of our data sets, the one presented in this paper is clearly superior in contrast and definition of detail. However, we are uncertain as to whether the data at 300 kV was collected under optimal conditions, e.g. aperture size.

An electron which passes through a specimen may be (1) unscattered, (2) elastically scattered, (3) inelastically scattered and (4) multiply scattered (Crewe & Groves, 1974). In a thin specimen stained with high  $Z$  number atoms, most electrons pass through unscattered, or are elastically scattered at high angles and trapped by the objective lens aperture. The relative absence of inelastically and multiply scattered electrons yields images which are sharp and free of chromatic aberration. When thicker specimens are studied a larger percentage of inelastically and multiply scattered electrons is observed resulting in chromatic aberrations, i.e. 'fuzzier' images. Increasing the energy ( $E_0$ ) of the electron beam has proved to be an effective way to decrease the number of inelastically and multiply scattered electrons (Turner, 1981; Olins *et al.*, 1986; McEwen *et al.*, 1986; Belmont *et al.*, 1987). The development of the scanning transmission electron microscope (STEM) was another development which permitted imaging of thicker sections. This microscope has no lenses beyond the specimen, the electrons are analysed electronically and thus the differences in their energy does not affect the image quality. Crewe & Groves (1974) suggest STEM can image specimens about five times thicker than CEM at the same voltage. Most recently, energy filtration (Castaing & Henry, 1962, 1964) has become commercially available (Zeiss EM902) and thick sections can be imaged clearly at 80 kV if only a small, energetically homogeneous portion of the electrons collected is used for imaging. The zero energy loss electrons (if available) or the electrons near or slightly below the spectrum maximum can be used to form high quality images. This method of decreasing chromatic aberration, i.e. imaging with electrons of fairly uniform energy, is practical and theoretically sound.

When thickness is expressed in terms of mean free path (i.e.  $x = t/\lambda$  where  $t$  is the thickness and  $\lambda$  is the mean free path), the parameters which alter the energy loss spectrum in a similar way are apparent. Increases in thickness due to sectioning or tilting, or changes in  $\lambda$  caused by decreased energy of the electron beam or by increased atomic number of the atoms in the specimen, lead to a decrease in zero loss electrons and a broadening and shift to higher energy loss of the multiply scattered electrons (Figs. 1 and 2). The thickness  $t$  of a specimen traversed by the electron beam is equal to  $t_0/\cos \alpha$  where  $t_0$  is the thickness of the section and  $\alpha$  is the angle of tilt. Figure 2

---

**Fig. 4.** Six sequential tomographic slices from the final reconstruction. The series begins with the upper left frame, moving across and terminates with the lower right frame. Each frame is  $512 \times 512 \times 2$  pixels; 1 pixel equals 10 nm. The contrast has been photographically reversed in this series, thus gold particles and chromatin loops are light structures on a dark background.

shows that, in a specimen where  $\lambda$  is constant, the value  $\Delta E_p$  is proportional to the thickness of the specimen presented to the electron beam. The absence of linearity of the last point on the curve is clearly due to the difficulty of determining the position of  $\Delta E_p$  on a very broad curve.

We have shown in a separate study (Colliex *et al.*, 1989) that contrast is optimal in bright field images formed by  $\Delta E = 0$  electrons. It is known (Pearce-Percy & Cowley, 1976) that contrast reversal can occur when images are formed with inelastically scattered electrons. It was therefore quite important for us to show that we were using electrons with energy losses well below the transition point between bright and dark field images. Our calculations showed that for samples of thickness  $x = 1$  and 2, the contrast is reversed at approximately  $\Delta E \cong 25$  eV (1 plasmon) and  $\Delta E \cong 75$  eV (3 plasmons), respectively. For such thin samples, however, the intensity of  $\Delta E = 0$  electrons is sufficiently high to form high contrast images without any danger of contrast reversal. For a specimen thickness  $x = 3$  (similar to that used in this reconstruction at  $\alpha = 0^\circ$ ) contrast reversal occurs at  $\Delta E \cong 210$  eV or 8.5 plasmons; our  $\alpha = 0^\circ$  images were obtained using  $125 \pm 10$  eV loss electrons. The signal to noise (S/N) ratio is optimal at about 0.5 plasmons (13 eV) below  $\Delta E_p$ , also a point well removed from the contrast reversal. Although we recommend the S/N ratio maximum as the first choice for optimal imaging conditions of a thick specimen (insufficient  $\Delta E = 0$  intensity for image formation), the condition used in the present study ( $\Delta E_p \pm 10$  eV) is sufficiently close to the S/N ratio maximum and sufficiently far from the point of contrast reversal that we feel quite confident in treating the images as normal bright field members of a tomographic tilt series.

Energy filtration, as a method for imaging thick sections, is a practical method for removing chromatic aberration and obtaining high contrast, sharp images. Future development of higher than 80 kV electron microscopes with energy filtration capabilities would, of course, extend these advantages to even thicker sections. The limitation imposed by local variations in  $x$  when average values of  $x$  are used to determine the imaging conditions should be explored.

Further studies of this tomogram will permit us to measure lengths of transcription units and possibly the position of individual transcripts along the chromatin axis.

#### ACKNOWLEDGMENTS

This study was funded by NSF grant PCM-8400537 to D.E.O. and A.L.O., NSF grant DCB-8501261 to A.L.O. and by the Office of Health and Environmental Research, U.S. Department of Energy under contract DE-AC05-84OR21400 with the Martin Marietta Energy Systems, Inc. The work reported in this paper was undertaken during the tenure of an American Cancer Society – Eleanor Roosevelt – International Cancer Fellowship awarded by the International Union Against Cancer to A.L.O. and a Scholar in Cancer Research Grant from the American Cancer Society to D.E.O. We thank Drs Hezel and Probst of Carl Zeiss, Oberkochen, for their help and hospitality. Critical reading of the manuscript by D. P. Allison and C. L. Cadilla is gratefully acknowledged. The biological specimens were prepared in the laboratory of Markus Lezzi, Zurich.

#### REFERENCES

- Bauer, R. (1987) High resolution imaging of thick biological specimens with an imaging electron energy loss spectrometer. *Zeiss-Inform. MEM. Oberkochen*, 5, 10–15.
- Belmont, A.S., Sedat, J.W. & Agard, D.A. (1987) A three-dimensional approach to mitotic chromosome structure: Evidence for a complex hierarchical organization. *J. Cell Biol.* 105, 77–92.
- Castaing, R. & Henry, L. (1962) Filtrage magnetique des vitesses en microscopie electronique. *C. R. Acad. Sci. Paris B.* 255, 76–78.
- Castaing, R. & Henry, L. (1964) Filtrage magnetique des vitesses en microscopie electronique. *J. Microscopie*, 3, 133–152.

- Colliex, C., Mory, C., Olins, A.L., Olins, D.E. & Tence, M. (1989) Energy filtered STEM imaging of thick biological sections. *J. Microsc.* **153**, 1–21.
- Crewe, A.V. & Groves, T. (1974) Thick specimens in the CEM and STEM I. *Contrast. J. Appl. Phys.* **45**, 3662–3672.
- DeRosier, D.J. & Klug, A. (1968) Reconstruction of three dimensional structures from electron micrographs. *Nature*, **217**, 130–134.
- Heath, J.P. & Peachy, L.D. (1987) Electron microscopy of thick sections of embedded cells using the Zeiss EM902 energy filtering electron microscope. *Zeiss-Inform. MEM, Oberkochen*, **5**, 15–21.
- Hoppe, W. & Hegerl, R. (1980) Three-dimensional structure determination by electron microscopy (non-periodic specimens). In: *Computer Processing of Electron Microscope Images* (ed. by P. W. Hakes), pp. 127–185. Springer-Verlag, Berlin.
- McEwen, B.F., Radermacher, M., Rieder, C.L. & Frank, J. (1986) Tomographic three-dimensional reconstruction of cilia ultrastructure from thick sections. *Proc. Natl. Acad. Sci. USA*, **83**, 9040–9044.
- Olins, A.L., Olins, D.E., Levy, H.A., Durfee, R.C., Margle, S.M. & Tinnel, E.P. (1986) DNA compaction during intense transcription measured by electron microscope tomography. *Eur. J. Cell Biol.* **40**, 105–110.
- Olins, A.L., Olins, D.E., Levy, H.A., Durfee, R.C., Margle, S.M., Tinnel, E.P., Hingerty, B.E., Dover, S.D. & Fuchs, H. (1984) Modeling balbiani ring gene transcription with electron microscope tomography. *Eur. J. Cell Biol.* **35**, 129–142.
- Olins, D.E., Olins, A.L., Levy, H.A., Durfee, R.C., Margle, S.M., Tinnel, E.P. & Dover, S.D. (1983) Electron microscope tomography: transcription in three dimensions. *Science*, **220**, 498–500.
- Pearce-Percy, H.T. & Cowley, J.M. (1976) On the use of energy filtering to increase the contrast of STEM images of thick biological materials. *Optik*, **44**, 273–288.
- Skoglund, U., Andersson, K., Strandberg, B. & Daneholt, B. (1986) Three-dimensional structure of a specific pre-messenger RNP particle established by electron microscope tomography. *Nature*, **319**, 560–564.
- Turner, J.N. (1981) Introduction to stereo imaging. In: *Three-dimensional Ultrastructure in Biology* (ed. by J. N. Turner) *Methods in Cell Biology*, Vol. 22, pp. 1–11. Academic Press, New York.